Appl. Phys. B (2014) 114:467–474
DOI 10.1007/s00340-013-5543-x

Applied Physics B
Lasers and Optics

Characterization of waveguide loss using distributed Bragg reflectors

Andrew Grieco · Boris Slutsky · Yeshaiahu Fainman

Received: 18 March 2013 / Accepted: 1 June 2013 / Published online: 14 June 2013

Abstract We propose and demonstrate a method to characterize waveguide loss using the spectral response of combinations of distributed Bragg reflectors. The method is independent of coupling efficiency and waveguide dispersion and does not require the introduction of bending loss into the device.

1 Introduction

Waveguide loss arises from a number of different sources, including scattering loss [1, 2], material absorption, and bending of the guide. Accurate estimation of waveguide loss is crucial to the design of some integrated photonic devices. For example, nonlinear devices are very sensitive to operating power. This is true in the sense that with too little power the device will not function and with too much power the device can become unstable [3].

The most direct methods of characterization involve the determination of total loss by comparing the transmission of waveguides of different lengths and the separation of input and output coupling loss from waveguide loss by linear regression [4]. However, in the case of low loss waveguides, the device length required to obtain an accurate loss measurement can be difficult to fabricate. It is possible to improve the device footprint by folding the waveguide, although this introduces bending losses which must be accounted for [5, 6]. Bending can also distort the mode profile and alter its susceptibility to scattering loss. In this situation, it cannot be presumed that the scattering loss is equivalent to that of the unbent guide. Creating consistent input and output coupling can also be problematic in small-scale devices.

A technique for determining waveguide loss using ring resonators also exists [7, 8]. In this method, it is possible to infer total loss from spectral characteristics of the resonator. Since the optical field circulates many times within the resonator, accurate loss measurements can be obtained from relatively compact devices. Additionally, the measurement is independent of input and output coupling. However, waveguide bending becomes unavoidable. Likewise, additional effort must be made during analysis to separate the loss coefficient from the power splitting coefficient of the ring coupler, since both appear identically in the resonator equations. Finally, additional analysis is required in the presence of waveguide dispersion.

A linear waveguide resonator formed by a pair of distributed Bragg reflectors (DBRs) can be used to characterize waveguide loss through fitting of the experimental spectra [9]. In this approach, waveguide bending loss is avoided, but the propagation loss cannot be distinguished from the reflection loss at the DBR, which is often comparable or greater than the loss in the straight waveguide section, may vary with wavelength, and may significantly depend on the fabrication quality of the DBR.

In this paper, we describe a method to characterize waveguide loss based on the comparison of the spectral responses of three DBR devices, in each case using a DBR reflectance null point as a reference. The method is independent of coupling efficiency, does not require the introduction of bending into the device, and makes no a priori assumptions with regard to DBR loss. As a result, only

A. Grieco (✉) · B. Slutsky · Y. Fainman
Department of Electrical and Computer Engineering, University of California, San Diego, 9500 Gilman Drive, San Diego, CA 92093, USA
e-mail: agrieco@ucsd.edu

B. Slutsky
e-mail: bslutsky@emerald.ucsd.edu

Y. Fainman
e-mail: yfainman@ucsd.edu

scattering loss and material absorption contribute to the measured loss. The method possesses the footprint advantage of resonant devices, and waveguide dispersion does not introduce errors. It is particularly useful for situations in which the bending necessitated by the alternative methods would degrade the loss estimate.

2 Theory

2.1 Spectral response of a distributed Bragg reflector

The reflectance of a distributed Bragg reflector created by the periodic perturbation of a dielectric waveguide may be described in the context of coupled-mode theory [10]. This formalism represents the permittivity profile $\varepsilon(x, y, z)$ of the periodic structure as the Fourier series: $\varepsilon(x, y, z) = \Sigma_m \varepsilon_m(x, y)\exp(-i{\cdot}m{\cdot}2\pi/\Lambda{\cdot}z)$, where Λ is the period of the perturbation and m is an integer. The full solution is then written as a combination of propagating modes of the z-invariant waveguide described by the term $\varepsilon_0(x, y)$ of the series. The effect of the perturbation is to transfer energy from one mode to another, mostly when the difference between the propagation constants of the modes equals or comes close to $m{\cdot}2\pi/\Lambda$ for some m. In Bragg reflectors, the two modes of interest are a forward propagating mode with propagation constant β_F and a reflected mode with propagation constant $-\beta_B$. The number of other propagating modes is usually limited, and their propagation constants are not matched to either β_F or $-\beta_B$ by any grating order m, allowing the coupling into these modes to be neglected (in a single mode waveguide, the only possible match is $\beta_F = \beta_B$). Energy coupled into radiating modes quickly leaves the guide and can be accounted for as propagation loss. With these assumptions, the differential equations that govern the mode amplitudes are [10]:

$$\frac{dA_F}{dz} = -i \cdot \kappa \cdot A_B \exp(i \cdot \Delta\beta \cdot z) - \frac{\alpha_{DBR}}{2} A_F \tag{1}$$

$$\frac{dA_B}{dz} = i \cdot \kappa^* \cdot A_F \exp(-i \cdot \Delta\beta \cdot z) + \frac{\alpha_{DBR}}{2} A_B \tag{2}$$

$$\Delta\beta = \beta_F - (-\beta_B) - m\frac{2\pi}{\Lambda} \tag{3}$$

where A_F and A_B are the respective amplitudes of the forward and backward propagating waves. The coupling coefficient κ is a function of the m-th Fourier series component $\varepsilon_m(x,y)$ of the perturbation and the extent to which it overlaps with the guided modes. The propagation distance within the DBR is indicated by z, α_{DBR} is the linear loss coefficient of the DBR, and β_F and $-\beta_B$ are the respective propagation constants of the forward and backward propagating modes. By decoupling the equations, the general solution may be determined to assume the form:

$$A_F = \exp\left(\frac{i \cdot \Delta\beta \cdot z}{2}\right) \cdot [C_1 \exp(s \cdot z) + C_2 \exp(-s \cdot z)] \tag{4}$$

$$A_B = \exp\left(\frac{-i \cdot \Delta\beta \cdot z}{2}\right) \cdot [D_1 \exp(s \cdot z) + D_2 \exp(-s \cdot z)] \tag{5}$$

$$s = \sqrt{\left(\kappa^*\kappa + i \cdot \Delta\beta \frac{\alpha_{DBR}}{2} + \frac{\alpha_{DBR}^2}{4}\right) - \left(\frac{\Delta\beta}{2}\right)^2} \tag{6}$$

where C_1, C_2, D_1, and D_2 are constants. Applying this result to a grating of length L_{DBR} with a forward propagating wave injected at $z = 0$ and no back propagating wave injected at $z = L_{DBR}$, i.e., such that $A_B(L_{DBR}) = 0$ and $A_F(0) \neq 0$, yields the coefficient of reflection r_F and coefficient of transmission t_F of the periodic structure:

$$r_F = \frac{A_B(0)}{A_F(0)} = \frac{-i \cdot \kappa^* \cdot L_{DBR}}{\frac{i \cdot \Delta\beta + \alpha_{DBR}}{2} \cdot L_{DBR} + \frac{s \cdot L_{DBR}}{\tanh(s \cdot L_{DBR})}} \tag{7}$$

$$t_F = \frac{A_F(L)}{A_F(0)} = \frac{\frac{s \cdot L_{DBR} \cdot \exp\left(i\frac{\Delta\beta}{2} \cdot L_{DBR}\right)}{\sinh(s \cdot L_{DBR})}}{\frac{i \cdot \Delta\beta + \alpha_{DBR}}{2} \cdot L_{DBR} + \frac{s \cdot L_{DBR}}{\tanh(s \cdot L_{DBR})}}. \tag{8}$$

The derivation of Eqs. (7) and (8) is provided in the "Appendix". The coefficient of reflection r_B and coefficient of transmission t_B for an input wave that is backward propagating at $z = L_{DBR}$ may be derived in a similar manner using the appropriate boundary conditions. In the absence of loss ($\alpha_{DBR} = 0$), Eqs. (7) and (8) reduce to the form commonly found in the literature [10].

The dependence of DBR reflectance and transmittance on spectral detuning $\Delta\beta$ in the absence of loss ($\alpha_{DBR} = 0$) is illustrated in Fig. 1. When $\alpha_{DBR} = 0$, the points $\Delta\beta = \pm 2|\kappa|$ give $s = 0$ in Eq. (6) and are conventionally defined as the edges of the stopband, although the reflectance is nonzero at these points:

$$\lim_{s\to 0} r_F = \frac{-i \cdot \kappa^* \cdot L_{DBR}}{\lim_{s\to 0} \frac{i \cdot \Delta\beta}{2} \cdot L_{DBR} + \lim_{s\to 0} \frac{s \cdot L_{DBR}}{\tanh(s \cdot L_{DBR})}} = \frac{-i \cdot \kappa^* \cdot L_{DBR}}{i|\kappa| \cdot L_{DBR} + 1} \neq 0 \quad (\alpha_{DBR} = 0). \tag{9}$$

However, true reflectance null points occur at $s{\cdot}L_{\mathrm{DBR}} = n{\cdot}i{\cdot}\pi$ for integers $n \neq 0$, where $\tanh(s{\cdot}L_{\mathrm{DBR}}) = 0$ but $s{\cdot}L_{\mathrm{DBR}} \neq 0$ and therefore $\lim(|s{\cdot}L_{\mathrm{DBR}}/\tanh(s{\cdot}L_{\mathrm{DBR}})|) = \infty$. The corresponding wavevector values are:

$$\Delta\beta_{\mathrm{null}} = \pm 2\sqrt{\kappa^{*}\kappa + \left(\frac{n\cdot\pi}{L_{\mathrm{DBR}}}\right)^{2}}, \quad n = 1, 2, \ldots \tag{10}$$

The maximum reflectance occurs at the band center $\Delta\beta = 0$. For a lossless grating, the maximum coefficient of reflection is $r_F(\Delta\beta = 0) = \tanh(\kappa{\cdot}L_{\mathrm{DBR}})$.

When loss is included, the reflectance at $\Delta\beta_{\mathrm{null}}$ is no longer zero, but remains small. To the first order in α_{DBR}, the magnitude of the coefficient of reflection at the null point is:

$$|r_F|_{\mathrm{null}} \approx \frac{(\alpha_{\mathrm{DBR}}\cdot L_{\mathrm{DBR}})(|\kappa|L_{\mathrm{DBR}})\sqrt{(|\kappa|L_{\mathrm{DBR}})^{2}+(n\cdot\pi)^{2}}}{2(n\cdot\pi)^{2}}. \tag{11}$$

The derivation of Eq. (11) is provided in the "Appendix". Since the periodic perturbation is an engineered structure, it is generally possible to construct a DBR with both high maximum reflectance (e.g., $|\kappa|L_{\mathrm{DBR}} = 2$) and vanishingly small reflectance at the $\Delta\beta_{\mathrm{null}}$ points. This property of Bragg reflectors is the basis of the waveguide loss characterization method proposed in the present work. Specifically, a point of vanishing reflectance will be exploited to normalize the transmission spectrums of different combinations of DBRs for comparison, which will ultimately allow the inference waveguide loss. Any of the null points $n = 1, 2, \ldots$ can be used for this purpose. Note that higher order nulls yield lower reflection in Eq. (11), but move the reference wavelength farther from the DBR stopband.

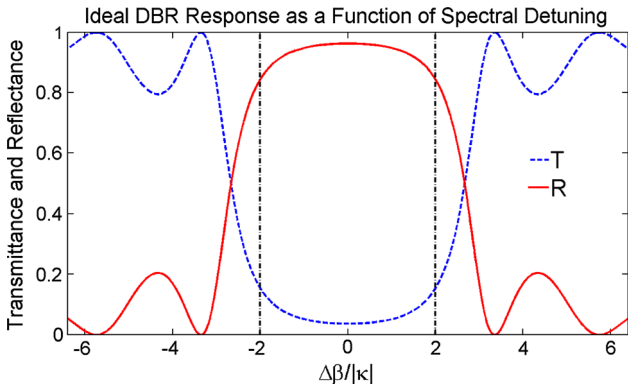

Fig. 1 Dependence of the response of an ideal DBR on spectral detuning. In this example, $|\kappa| = 600\ \mathrm{cm}^{-1}$ and $L_{\mathrm{DBR}} = 38.912\ \mu\mathrm{m}$. *Vertical lines* denote the conventional edge of the stopband

2.2 Distributed Bragg reflector Fabry–Pérot resonator

The transmittance of a Fabry–Pérot resonator formed by a pair of DBRs is given by the equation:

$$T_{FP}(\lambda) = \frac{|t_{F,1}(\lambda)|^{2}|t_{F,2}(\lambda)|^{2}\exp(-\alpha\cdot L_{\mathrm{cav}})}{\left|1 - r_{B,1}(\lambda)\cdot r_{F,2}(\lambda)\exp[-2i\cdot\phi(\lambda)]\exp(-\alpha\cdot L_{\mathrm{cav}})\right|^{2}} \tag{12}$$

where T_{FP} is the resonator transmittance, α is the cavity power loss coefficient, L_{cav} is the resonance cavity length, and φ is the phase shift of the field upon traversing the cavity [11]. The subscripts 1 and 2 associated with the DBR coefficients of transmission and reflection refer, respectively, to the first and second DBR of the resonator, as they need not be identical. In the case of a linear waveguide, the parameter φ is given by:

$$\phi(\lambda) = \frac{2\pi\cdot n_{\mathrm{eff}}(\lambda)\cdot L_{\mathrm{cav}}}{\lambda} \tag{13}$$

where n_{eff} is the effective index of the guided mode, and λ is the free space wavelength of the guided light.

We first apply Eq. (12) to a DBR resonator with a short cavity, e.g., one DBR period in length. In this arrangement, the loss in the cavity will be negligible compared to the loss from the reflective elements, since the DBR elements are many periods in length. Consequently, the equation for resonator transmittance reduces to:

$$T_{FP,SC}(\lambda) = \frac{|t_{F,1}(\lambda)|^{2}|t_{F,2}(\lambda)|^{2}}{\left|1 - r_{B,1}(\lambda)\cdot r_{F,2}(\lambda)\exp[-2i\cdot\phi(\lambda)]\right|^{2}}. \tag{14}$$

From this, we may make two important observations. First, the transmittance at the reflectance null point $\Delta\beta_{\mathrm{null}}$ is:

$$\begin{aligned} T_{FP,SC}(\lambda_{\mathrm{null}}) &= |t_{F,1}(\lambda_{\mathrm{null}})|^{2}|t_{F,2}(\lambda_{\mathrm{null}})|^{2} \\ &= T_{\mathrm{DBR},1}(\lambda_{\mathrm{null}})T_{\mathrm{DBR},2}(\lambda_{\mathrm{null}}) \end{aligned} \tag{15}$$

where T_{DBR} is the transmittance of the individual DBR elements, with subscripts indicating order of occurrence as before. Second, at the cavity resonance, the resonator transmittance equals:

$$T_{FP,SC}(\lambda_{SC,\mathrm{res}}) = \frac{|t_{F,1}(\lambda_{SC,\mathrm{res}})|^{2}|t_{F,2}(\lambda_{SC,\mathrm{res}})|^{2}}{\left[1 - |r_{B,1}(\lambda_{SC,\mathrm{res}})\cdot r_{F,2}(\lambda_{SC,\mathrm{res}})|\right]^{2}}. \tag{16}$$

If we divide the expression for resonance transmittance Eq. (16) by the null point transmittance Eq. (15), we arrive at the relationship:

$$\frac{T_{FP,SC}(\lambda_{SC,\mathrm{res}})}{T_{FP,SC}(\lambda_{\mathrm{null}})} = \frac{|t_{F,1}(\lambda_{SC,\mathrm{res}})|^2 |t_{F,2}(\lambda_{SC,\mathrm{res}})|^2}{|t_{F,1}(\lambda_{\mathrm{null}})|^2 |t_{F,2}(\lambda_{\mathrm{null}})|^2 [1 - |r_F(\lambda_{SC,\mathrm{res}}) \cdot r_B(\lambda_{SC,\mathrm{res}})|]^2}. \quad (17)$$

The product of DBR reflection coefficients at resonance may be expressed explicitly by rearranging Eq. (17):

$$|r_{B,1}(\lambda_{SC,\mathrm{res}}) \cdot r_{F,2}(\lambda_{SC,\mathrm{res}})| = 1 - \sqrt{\frac{T_{\mathrm{DBR},1}(\lambda_{SC,\mathrm{res}})}{T_{\mathrm{DBR},1}(\lambda_{\mathrm{null}})}} \sqrt{\frac{T_{\mathrm{DBR},2}(\lambda_{SC,\mathrm{res}})}{T_{\mathrm{DBR},2}(\lambda_{\mathrm{null}})}} \sqrt{\frac{T_{FP,SC}(\lambda_{\mathrm{null}})}{T_{FP,SC}(\lambda_{SC,\mathrm{res}})}}. \quad (18)$$

Equation (18) gives the product of DBR reflection coefficients $|r_{B,1}(\lambda_{SC,\mathrm{res}}) \cdot r_{F,2}(\lambda_{SC,\mathrm{res}})|$ at the resonance wavelength of the short cavity in terms of power transmittance ratios, namely $T_{\mathrm{DBR},1}(\lambda_{SC,\mathrm{res}})/T_{\mathrm{DBR},1}(\lambda_{\mathrm{null}})$, $T_{\mathrm{DBR},2}(\lambda_{SC,\mathrm{res}})/T_{\mathrm{DBR},2}(\lambda_{\mathrm{null}})$ and $T_{FP,SC}(\lambda_{\mathrm{null}})/T_{FP,SC}(\lambda_{SC,\mathrm{res}})$. The former two can be determined from the measured transmittance spectrum of the individual DBR elements, and the latter from the transmittance spectrum of the short cavity. All the ratios are independent of waveguide coupling loss and of any loss in the guide sections leading in and out of the test structures.

With the knowledge of the DBR reflection coefficients, it is possible to infer waveguide loss using a resonator with a long cavity. In this arrangement, the cavity loss is no longer negligible. From Eq. (12), the resonator transmittance at the null point is thus:

$$T_{FP,LC}(\lambda_{\mathrm{null}}) = |t_{F,1}(\lambda_{\mathrm{null}})|^2 |t_{F,2}(\lambda_{\mathrm{null}})|^2 \exp(-\alpha \cdot L_{\mathrm{cav}}) = T_{\mathrm{DBR},1}(\lambda_{\mathrm{null}}) T_{\mathrm{DBR},2}(\lambda_{\mathrm{null}}) \exp(-\alpha \cdot L_{\mathrm{cav}}). \quad (19)$$

Likewise, at each long cavity resonance, the transmittance equals:

$$T_{FP,LC}(\lambda_{LC,\mathrm{res}}) = \frac{|t_{F,1}(\lambda_{LC,\mathrm{res}})|^2 |t_{F,2}(\lambda_{LC,\mathrm{res}})|^2 \exp(-\alpha \cdot L_{\mathrm{cav}})}{[1 - |r_{B,1}(\lambda_{LC,\mathrm{res}}) \cdot r_{F,2}(\lambda_{LC,\mathrm{res}})| \exp(-\alpha \cdot L_{\mathrm{cav}})]^2}. \quad (20)$$

If we follow a similar procedure as before and divide the expression for resonance transmittance in the long cavity case Eq. (20) by the null point transmittance Eq. (19), we arrive at the relationship:

$$\frac{T_{FP,LC}(\lambda_{LC,\mathrm{res}})}{T_{FP,LC}(\lambda_{\mathrm{null}})} = \frac{|t_{F,1}(\lambda_{LC,\mathrm{res}})|^2 |t_{F,2}(\lambda_{LC,\mathrm{res}})|^2}{|t_{F,1}(\lambda_{\mathrm{null}})|^2 |t_{F,2}(\lambda_{\mathrm{null}})|^2 [1 - |r_{B,1}(\lambda_{LC,\mathrm{res}}) \cdot r_{F,2}(\lambda_{LC,\mathrm{res}})| \exp(-\alpha \cdot L_{\mathrm{cav}})]^2}. \quad (21)$$

It is generally possible to choose the long cavity length L_{cav} so that one of its resonances coincides with one of the resonances of the short cavity. For example, if both cavity lengths are integer multiples of the DBR period, each cavity will have a resonance at the exact center of the stopband. For these coincident resonances, $\lambda_{LC,\mathrm{res}} = \lambda_{SC,\mathrm{res}} = \lambda_{\mathrm{res}}$, and the product of the DBR coefficients of reflection $|r_{B,1}(\lambda_{\mathrm{res}}) \cdot r_{F,2}(\lambda_{\mathrm{res}})|$ appearing in Eq. (21) is known from Eq. (18). Equation (21) is thus readily solved for the loss factor. Substituting in the prior expression for the DBR coefficients of reflection Eq. (18), the cavity loss at resonance may be expressed as:

$$\exp(-\alpha \cdot L_{\mathrm{cav}}) = \frac{1 - \sqrt{\frac{T_{\mathrm{DBR},1}(\lambda_{\mathrm{res}})}{T_{\mathrm{DBR},1}(\lambda_{\mathrm{null}})}} \sqrt{\frac{T_{\mathrm{DBR},2}(\lambda_{\mathrm{res}})}{T_{\mathrm{DBR},2}(\lambda_{\mathrm{null}})}} \sqrt{\frac{T_{FP,LC}(\lambda_{\mathrm{null}})}{T_{FP,LC}(\lambda_{\mathrm{res}})}}}{1 - \sqrt{\frac{T_{\mathrm{DBR},1}(\lambda_{\mathrm{res}})}{T_{\mathrm{DBR},1}(\lambda_{\mathrm{null}})}} \sqrt{\frac{T_{\mathrm{DBR},2}(\lambda_{\mathrm{res}})}{T_{\mathrm{DBR},2}(\lambda_{\mathrm{null}})}} \sqrt{\frac{T_{FP,SC}(\lambda_{\mathrm{null}})}{T_{FP,SC}(\lambda_{\mathrm{res}})}}}. \quad (22)$$

Placing λ_{res} near the center of the stopband is particularly advantageous because DBR properties at band center are less sensitive to small frequency errors. Eq. (22) is the primary result of this paper.

3 Experimental demonstration

3.1 Fabrication and characterization

The simplest manifestation of Eq. (22) occurs for the case of a symmetrical resonator in which the DBR elements are identical. In such an arrangement, the waveguide loss may be identified from three transmittance ratios: $T_{\mathrm{DBR}}(\lambda_{\mathrm{res}})/T_{\mathrm{DBR}}(\lambda_{\mathrm{null}})$, $T_{FP,SC}(\lambda_{\mathrm{null}})/T_{FP,SC}(\lambda_{\mathrm{res}})$, and $T_{FP,LC}(\lambda_{\mathrm{null}})/T_{FP,LC}(\lambda_{\mathrm{res}})$. These can be obtained experimentally from the transmittance spectra of three structures: a single DBR, a pair of DBRs separated by a short cavity, and a pair of DBRs separated by a relatively long cavity, respectively. To illustrate the utility of this approach, these devices were fabricated in silicon strip waveguides. The fabrication and characterization techniques have been described previously [12]. In brief, the devices are created from a 250 nm silicon-on-insulator (SOI) substrate with a 3 μm buried oxide layer. The substrate is patterned with a hydrogen silsesquioxane (HSQ) mask via electron beam lithography. The substrate then undergoes an inductively coupled plasma reactive-ion etch process, and the patterned silicon is then cladded with a layer of silicon dioxide deposited via plasma-enhanced chemical vapor deposition. All three devices were fabricated together on the same sample to minimize the random fabrication variations between the nominally identical DBRs.

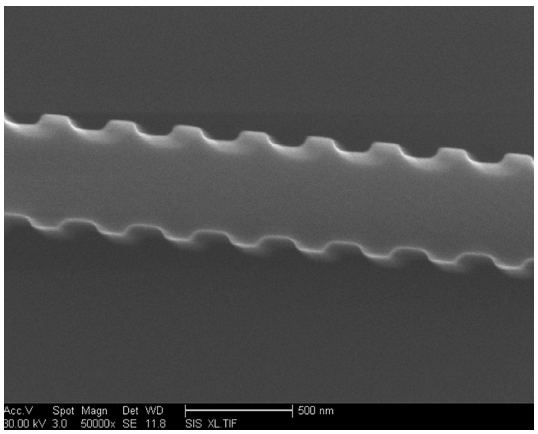

Fig. 2 Scanning electron micrograph of an uncladded section of DBR. Note that the *scale bar* label is 500 nm

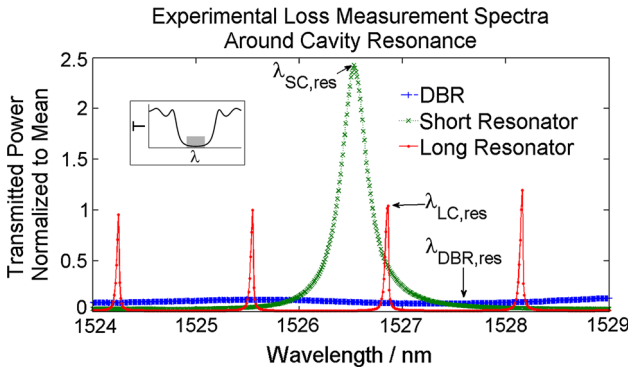

Fig. 3 Transmission spectra of the experimental structures about the cavity resonance. The *inset* in the *upper left* of the figure is a conceptual illustration in which the *shaded* area indicates the approximate position of the measurements relative to the DBR stopband

The nominal dimensions of the waveguide are 250 nm height and 500 nm width. The DBRs are formed by periodically modulating the waveguide width by ±50 nm (Fig. 2). The grating period is nominally 0.304 μm, and the DBRs are 90 periods long. The short resonance cavity is one grating period in length, and the long resonance cavity is 658 DBR periods in length. Parabolic inverse tapered couplers, narrowing to 134 nm at the tip, are employed at both the input and output terminals of the device.

Characterization of the device was performed using a tunable laser source (Agilent model 81980A) to excite the TE mode in the silicon waveguide, coupled using a lensed tapered fiber. Transmitted light is collected by a microscope objective. A polarizer is used to reject any TM mode component that may arise from imperfect alignment of the lensed fiber. The detector used is Newport model 918D-IG-OD3, and the power meter used is Newport model 2931-C. Measurements are automated by a computer. For the measurements presented in this paper, the power registered

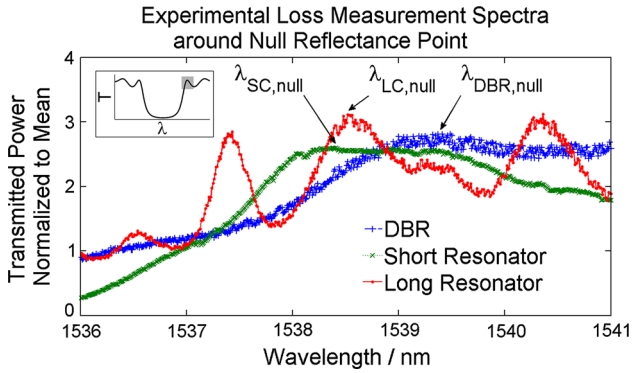

Fig. 4 Transmission spectra of the experimental structures about the null reflectance point. The *inset* in the *upper left* of the figure is a conceptual illustration in which the *shaded* area indicates the approximate position of the measurements relative to the DBR stopband

by the detector is corrected for the wavelength dependence of the laser output. The transmittance plots in Figs. 3 and 4 are normalized by the mean value of the spectra. This facilitates the presentation of the measurements on a common scale and is referred to as transmitted power normalized to mean. The normalization does not affect transmittance ratios entering Eq. (22).

3.2 Results

The normalized transmission spectra of the three structures about the resonance and null wavelengths are presented in Figs. 3 and 4. In the fabricated devices, the resonances and null points of the devices do not exactly coincide (e.g., $\lambda_{LC,\mathrm{res}} \neq \lambda_{SC,\mathrm{res}}$). The relative separation of the null point and resonance wavelengths, $\lambda_{\mathrm{res}} - \lambda_{\mathrm{null}}$, for each of the different structures differs by $\leq$0.15 nm. This is much smaller than the absolute separation between devices and suggests that the variation is due primarily to drift of the laboratory temperature between measurements. This is because the entire stopband shifts with changes in the laboratory temperature (as opposed to local heating of the cavity or fabrication error which would shift only the resonances). The offset has the potential to introduce error when the DBR coefficients of reflection at $\lambda_{SC,\mathrm{res}}$ from Eq. (17) are inserted for the reflection at $\lambda_{LC,\mathrm{res}}$ in Eq. (20). This error is small, however, because the DBR stopband is $\sim$20 nm wide and according to Eq. (7) the quantity $|r_{B,1}(\lambda_{\mathrm{res}})\cdot r_{F,2}(\lambda_{\mathrm{res}})|$ near the center of the stopband varies little ($\sim$0.001 %) over a 0.15 nm wavelength interval. This translates into a $\sim$0.07 % error in the loss estimate. The normalized power values at the points of interest are: $T_{\mathrm{DBR}}(\lambda_{\mathrm{null}}) = 2.81$ (at $\lambda = 1539.37$ nm), $T_{\mathrm{DBR}}(\lambda_{\mathrm{res}}) = 0.0805$ (at $\lambda = 1527.59$ nm), $T_{FP,SC}(\lambda_{\mathrm{null}}) = 2.59$ (at $\lambda = 1538.38$ nm), $T_{FP,SC}(\lambda_{\mathrm{res}}) = 2.43$ (at $\lambda = 1526.53$ nm), $T_{FP,LC}(\lambda_{\mathrm{null}}) = 3.10$ (at $\lambda = 1538.56$ nm), and

$T_{FP,LC}(\lambda_{res}) = 1.04$ (at $\lambda = 1526.86$ nm). The uncertainty in each power measurement is ± 3 %, and the propagation of this uncertainty in Eq. (22) may be calculated analytically [13]. The measured waveguide loss is therefore 4.5 ± 0.6 dB/cm (equivalently 1.0 ± 0.1/cm). This agrees well with the loss in nominally identical waveguides estimated by the fitting method [12].

3.3 Discussion

The proposed method of loss characterization has a number of distinct advantages. Since transmittance ratios are the only measurement involved, the method is independent of absolute coupling efficiency, which is particularly subject to fabrication uncertainty and can be difficult to characterize. The method does not require the introduction of bending loss or mode distortion into the device. The method is resonant and therefore possesses a footprint advantage over nonresonant methods, since it is possible to accumulate a larger total amount of loss over a smaller length of waveguide. Furthermore, the method is not degraded by waveguide dispersion, which only shifts the relative position of the relevant spectral features. The limitations of the method should also be explicitly considered, however.

It is necessary that the absolute coupling efficiency does not drift over the measurement time, otherwise error will be introduced into the power ratio measurements. For the same reason, it is also necessary that the device input and output coupling efficiency be the same at the null points $\Delta\beta_{null}$ and at the resonance point near $\Delta\beta = 0$. These limitations are generally easy to satisfy. Finally, it is necessary for the waveguide loss also to be identical at $\Delta\beta_{null}$ and $\Delta\beta = 0$. In practice, this condition will be met in most dielectric waveguides, except near points of material absorption lines. Note that it is not necessary for the DBR loss to be identical, or even similar, at $\Delta\beta_{null}$ and $\Delta\beta = 0$.

The error in the proposed loss characterization scheme will be dominated by three main sources. The first source is the noise floor of the measurement system, which can become significant if the DBRs are highly reflective and its transmittance at stopband center $T_{DBR}(\lambda_{res})$ is low. If this situation occurs, it will be impossible to accurately calculate the transmission ratios used to determine DBR reflectance and power loss. This problem can usually be avoided by the use of DBRs with lower reflectance and/or higher input powers. In the experiment reported here, the DBR rejection at stopband center is 16 dB, coupling loss (mostly on the fiber side) is 16 dB, and 6 dBm laser input power was used, producing -26 dBm power at the detector, well above detector noise floor of -50 dBm.

The second source of experimental error is impedance mismatch at the input and output coupling points at the facets of the sample. If the impedance mismatch is high, the coupling points themselves will act as additional mirrors, and the entire device will act as a series of coupled resonators. This will produce very complex transmission spectra and in general spoil the desired ratio measurements. The effect would be clearly visible, however, particularly on the transmittance spectra of a single DBR. In our experiment, inverse tapers were sufficient to suppress facet reflections. In the spectra shown in Fig. 4, any features due to reflections at coupling points are masked by other noise sources and need not be considered separately. If such features do appear, reflections can be further reduced by cleaving the facet at an angle to the waveguides, but this could complicate fabrication and reduce coupling efficiency. Increasing the distance between the couplers may also mitigate this effect by damping the unwanted outer resonator; however, it will increase the total device footprint.

The third source of error is fabrication process variations, leading to unintended differences between the resonator structures. If the propagation loss incurred over the cavity length L_{cav} is very small, reflectance variation among nominally identical DBRs could compromise the measurement. The gratings in this experiment were fabricated using electron beam lithography which results in a high degree of uniformity. Our measurements of similarly prepared resonators suggest that two nominally identical devices separated by 1 mm distance on the chip may differ by ~ 2 % in full width at half maximum, which would translate into ~ 0.07 % error in the quantity $|r_{B,1}(\lambda_{res}) \cdot r_{F,2}(\lambda_{res})|$ and ~ 3 % error in the loss estimate. This variation is a consequence of a number of causes, including drift of the electron beam path and focusing, and nonuniformity in the height of the SOI wafer and lithography resist. As such, it will increase with larger grating separation and longer pattern write times. Appropriate consideration during the design stage can generally minimize the impact of these effects. In the work presented here, the error is expected to be significantly less than 3 % because the devices were separated by less than 260 μm. Fabrication errors may also alter the optical path lengths of the resonator cavities and shift the position of the resonant peaks of the measurement devices relative to one another, resulting in $\lambda_{SC,res} \neq \lambda_{LC,res}$. However, as we have seen in Sect. 3.2, the first-order change in DBR parameters at the center of the stopband is very small, so a device engineered with a broad stopband will be resistant to this source of error. In the worst-case scenario, multiple devices of each type may be fabricated and the best matching pair used for measurement. The fabrication uncertainty in the cavity length is ~ 0.3 %, which has a negligible error contribution compared to the measurement uncertainty.

4 Conclusion

In conclusion, we have proposed and demonstrated a method to characterize waveguide loss using the spectral response of combinations of distributed Bragg reflectors. The method is independent of coupling efficiency and waveguide dispersion. It is conditional upon a small number of limitations that are easily met in practice, specifically that the coupling must be time independent, and the coupling and waveguide loss must be wavelength independent at the measurement points. It does not require the introduction of bending into the device and thereby avoids the introduction of bending loss into the device. Likewise, it avoids alteration of the mode susceptibility to scattering loss. As such, it serves as a complement to existing techniques.

Acknowledgments This work was supported by the National Science Foundation (NSF), the NSF Engineering Research Center for Integrated Access Networks, Defense Advanced Research Projects Agency, and the Cymer Corporation. The authors would like to thank the Nano3 staff at UCSD for support during sample fabrication, and C. Hennessey for logistical support.

Appendix: Derivations

Coefficients of transmission and reflection of a DBR

We shall take as our starting point Eqs. (1, 3) of the paper. To uncouple the equations, first differentiate them:

$$\frac{d^2A_F}{dz^2} = -i\cdot\kappa\cdot\frac{dA_B}{dz}\exp(i\cdot\Delta\beta\cdot z) + \kappa\cdot\Delta\beta\cdot A_B\exp(i\cdot\Delta\beta\cdot z) - \frac{\alpha_{DBR}}{2}\frac{dA_F}{dz} \tag{23}$$

$$\frac{d^2A_B}{dz^2} = i\cdot\kappa^*\cdot\frac{dA_F}{dz}\exp(-i\cdot\Delta\beta\cdot z) + \kappa^*\cdot\Delta\beta\cdot A_F\exp(-i\cdot\Delta\beta\cdot z) + \frac{\alpha_{DBR}}{2}\frac{dA_B}{dz} \tag{24}$$

Complete the decoupling by substitution from Eqs. (1, 3) in order to obtain separate differential equations for the forward and backward propagating field amplitudes:

$$\frac{d^2A_F}{dz^2} = \left(\kappa^*\kappa + i\cdot\Delta\beta\frac{\alpha_{DBR}}{2} + \frac{\alpha_{DBR}^2}{4}\right)A_F + i\cdot\Delta\beta\frac{dA_F}{dz} \tag{25}$$

$$\frac{d^2A_B}{dz^2} = \left(\kappa^*\kappa + i\cdot\Delta\beta\frac{\alpha_{DBR}}{2} + \frac{\alpha_{DBR}^2}{4}\right)A_B - i\cdot\Delta\beta\frac{dA_B}{dz} \tag{26}$$

The general solution of Eqs. (25, 26) is Eqs. (4–6) of the paper.

The boundary conditions that we will apply to determine the undetermined coefficients C_1, C_2, D_1, and D_2 in Eqs. (4–6) are $A_B(L_{DBR}) = 0$ and $A_F(0) =$ a nonzero constant. This corresponds to the physical arrangement in which only a forward propagating field is incident upon the DBR. It is possible to eliminate two of the coefficients by substituting the boundary conditions into Eqs. (4, 5). The general solutions may then be rewritten as:

$$A_F = 2\cdot C_1\cdot\exp\left(\frac{i\cdot\Delta\beta\cdot z}{2}\right)\sinh(s\cdot z) + A_F(0)\cdot\exp\left(\frac{i\cdot\Delta\beta\cdot z}{2}\right)\exp(-s\cdot z) \tag{27}$$

$$A_B = 2\cdot D_1\cdot\exp(s\cdot L_{DBR})\cdot\exp\left(\frac{-i\cdot\Delta\beta\cdot z}{2}\right)\sinh[s(z-L_{DBR})]. \tag{28}$$

Substituting Eqs. (27, 28) into Eqs. (1, 2) and again employing the boundary conditions, the remaining coefficients may be determined:

$$C_1 = \frac{\left(s - \frac{i\cdot\Delta\beta+\alpha_{DBR}}{2}\right)A_F(0)\exp(-s\cdot L_{DBR})}{(i\cdot\Delta\beta+\alpha_{DBR})\sinh(s\cdot L_{DBR}) + 2\cdot s\cdot\cosh(s\cdot L_{DBR})} \tag{29}$$

$$D_1 = \frac{-i\cdot\kappa^*\cdot A_1(0)\cdot\exp(-s\cdot L_{DBR})}{(i\cdot\Delta\beta+\alpha_{DBR})\sinh(-s\cdot L_{DBR}) - 2\cdot s\cdot\cosh(-s\cdot L_{DBR})}. \tag{30}$$

The coefficients of reflection and transmission may be determined by substituting Eqs. (29, 30) into Eqs. (27, 28):

$$r_F = \frac{A_B(0)}{A_F(0)} = \frac{-i\cdot 2\cdot\kappa^*\cdot\sinh(-s\cdot L_{DBR})}{(i\cdot\Delta\beta+\alpha_{DBR})\sinh(-s\cdot L_{DBR}) - 2\cdot s\cdot\cosh(-s\cdot L_{DBR})} \tag{31}$$

$$t_F = \frac{A_F(L)}{A_F(0)} = \frac{2\cdot s\cdot\exp\left(i\frac{\Delta\beta}{2}\cdot L_{DBR}\right)}{(i\cdot\Delta\beta+\alpha_{DBR})\sinh(s\cdot L_{DBR}) + 2\cdot s\cdot\cosh(s\cdot L_{DBR})} \tag{32}$$

where r_F is the coefficient of reflection and t_F is the coefficient of transmission. It is trivial to manipulate Eqs. (31, 32) into Eqs. (7, 8).

First-order approximation of null point coefficient of reflection

To arrive at the null point reflectance to first order in α_{DBR}, begin by considering the parameter s described by Eq. (6)

at the null point $\Delta\beta_{\text{null}}$ described by Eq. (10). Neglecting the term that is second order in α_{DBR}, the product $s{\cdot}L_{\text{DBR}}$ at such a point becomes:

$$s \cdot L_{\text{DBR}} \approx \sqrt{-(n \cdot \pi)^2 + i \cdot \Delta\beta_{\text{null}} \frac{\alpha_{\text{DBR}}}{2} \cdot L_{\text{DBR}}^2}. \tag{33}$$

Next, take the Taylor series of the radical in Eq. (33) and keep the terms to first order in α_{DBR}:

$$\begin{aligned} s \cdot L_{\text{DBR}} &\approx n \cdot i\pi \left(1 - \frac{i \cdot \Delta\beta_{\text{null}} \cdot \alpha_{\text{DBR}} \cdot L_{\text{DBR}}^2}{4(n \cdot \pi)^2}\right) \\ &= n \cdot i\pi + \frac{\Delta\beta_{\text{null}} \cdot \alpha_{\text{DBR}} \cdot L_{\text{DBR}}^2}{4 \cdot n \cdot \pi}. \end{aligned} \tag{34}$$

Next use the approximation in Eq. (34) to simplify the term in the denominator of coefficient of reflectance Eq. (7) containing the hyperbolic tangent:

$$\frac{s \cdot L_{\text{DBR}}}{\tanh(s \cdot L_{\text{DBR}})} \approx \frac{n \cdot i\pi}{\tanh\left(n \cdot i\pi + \frac{\Delta\beta_{\text{null}} \cdot \alpha_{\text{DBR}} \cdot L_{\text{DBR}}^2}{4 \cdot n \cdot \pi}\right)}. \tag{35}$$

Taking the hyperbolic tangent to first order and substituting in Eq. (10), Eq. (35) becomes:

$$\begin{aligned} \frac{s \cdot L_{\text{DBR}}}{\tanh(s \cdot L_{\text{DBR}})} &\approx \frac{n \cdot i\pi}{\frac{\Delta\beta_{\text{null}} \cdot \alpha_{\text{DBR}} \cdot L_{\text{DBR}}^2}{4 \cdot n \cdot \pi}} \\ &= \frac{\pm 2 \cdot i \cdot n^2 \cdot \pi^2}{\alpha_{\text{DBR}} \cdot L_{\text{DBR}} \sqrt{\kappa^* \kappa \cdot L_{\text{DBR}}^2 + (n \cdot \pi)^2}}. \end{aligned} \tag{36}$$

Substituting Eqs. (36) and (10) into Eq. (6) and keeping only terms of the first order in α_{DBR} results in the expression for reflectance:

$$r_F = \frac{\mp(\alpha_{\text{DBR}} \cdot L_{\text{DBR}})(\kappa^* \cdot L_{\text{DBR}})\sqrt{\kappa^* \kappa \cdot L_{\text{DBR}}^2 + (n \cdot \pi)^2}}{2 \cdot n^2 \cdot \pi^2}. \tag{37}$$

It is trivial to verify that taking the magnitude of Eq. (37) results in Eq. (11).

References

1. D. Marcuse, Bell Sys. Tech. J. **48**, 3187–3215 (1969)
2. F.P. Payne, J.P.R. Lacey, Opt. Quant. Electron. **26**, 977–986 (1994)
3. G.P. Agrawal, *Nonlinear Fiber Optics*, 4th edn. (Academic Press, New York, 2003)
4. P. Dong, W. Qian, S. Liao, H. Liang, C.-.C. Kung, N.-.N. Feng, R. Shafiiha, J. Fong, D. Feng, A.V. Krishnamoorthy, M. Asghari, Opt. Express **18**, 14474–14479 (2010)
5. M. Heiblum, IEEE J. Quantum Electron. **QE-11**, 75–83 (1975)
6. D.M. Shyroki, IEEE Trans. Microwave Theory Tech. **56**, 414–419 (2008)
7. A. Yariv, Electron. Lett. **4**, 321–322 (2000)
8. W.R. McKinnon, D.-X. Xu, C. Storey, E. Post, A. Densmore, A. Delâge, P. Waldron, J.H. Schmidt, S. Janz, Opt. Express **17**, 18971–18982 (2009)
9. Y. Painchaud, M. Poulin, C. Latrasse, M.-J. Picard, Bragg grating based Fabry-Perot filters for characterizing silicon-on-insulator waveguides. Paper presented at the IEEE 9th international conference on group IV photonics (GFP), San Diego, California, USA, 29–31 Aug. (2012)
10. A. Yariv, P. Yeh, *Optical Waves in Crystals: Propagation and Control of Laser Radiation* (Wiley, Hoboken, New Jersey 2003), Chap. 11
11. P. Yeh, *Optical Waves in Layered Media* (Wiley, Hoboken, New Jersey 2005), Chap. 6
12. H.-C. Kim, K. Ikeda, Y. Fainman, J. Lightw. Technol. **25**, 1147–1151 (2007)
13. J.R. Taylor, *An Introduction to Error Analysis: The Study of Uncertainties in Physical Measurements* (University Science Books, Sausalito, California 1997)